Journal Name

ARTICLE TYPE

Cite this: DOI: 00.0000/xxxxxxxxxx

Symmetry Lowering Through Surface Engineering and Improved Thermoelectric Properties in MXenes

Himanshu Murari[a], Subhradip Ghosh*[a]

Received Date
Accepted Date

DOI: 00.0000/xxxxxxxxxx

Supporting Information

1 Structural Models of Janus MXenes and Their Energetics

Fig. S1 shows the possible sites of surface passivation by functional groups in M_2C and MM′C Janus MXenes. The possible sites for functionalization are C (above and below the C atom), H (hollow sites above and below the transition metal atom), and T (exactly above the transition metal atom). Thus there are 9 possible structural models for functionalized Janus MXenes.

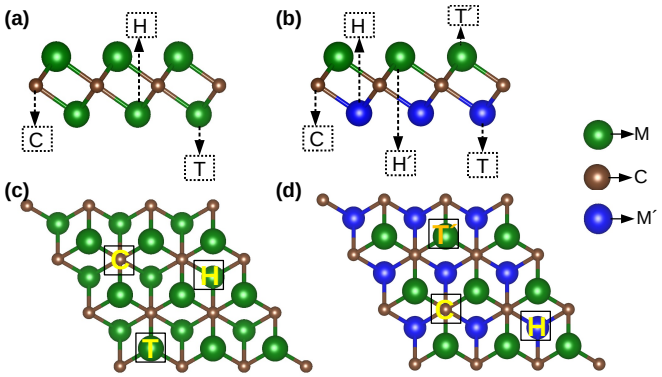

Fig. S1 Schematic diagram showing the possible sites of surface passivation in M_2C ((a): side view, (c): top view) and MM′C MXenes ((b): side view, (d): top view).

In Table S1, the total energies of all models for each one of the five Janus MXenes considered in the work, are shown. Results for non-degenerate structural models are shown only. While Mo-containing Janus compounds have -O preferring a HC combination, for the non-Mo ones it is HH (Fig. S2).

Models(MD)	Energy (eV)				
	$TiMoCO_2$	$ZrMoCO_2$	$HfMoCO_2$	$TiZrCO_2$	$TiHfCO_2$
MD1 (TT′)	-43.8985	-44.3654	-46.9871	-44.8060	-46.5082
MD2 (HH′)	-45.4814	-45.9024	-47.7030	**-45.3306**	**-47.2035**
MD3 (CH′)	-44.7065	-45.4717	-47.0970	-44.5926	-46.5123
MD4 (CC)	-45.0784	-45.5988	-47.5484	-43.8902	-45.5739
MD5 (HC)	**-45.9870**	**-46.4794**	**-48.3104**	-44.8059	-46.4587

Table S1 Total energy (eV) of different structural models for all Janus-MXenes considered in this work. The lowest energy in each case is shown in bold.

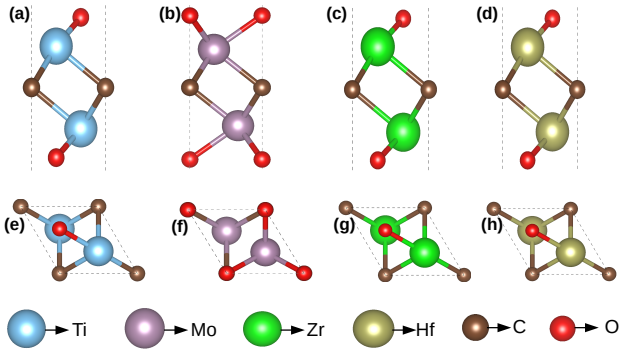

Fig. S2 Ground state structures of M_2CO_2 MXenes considered in this work. The top(bottom) row shows side(top) views of the systems.

2 Electronic Structures

Fig. S3 shows the calculated electronic band structure of the M_2CO_2 MXenes considered in this work. Except Mo_2CO_2, other three are semiconductors. The band gap gradually increases as the Group IV element in the MXene becomes heavier. The band structures of Zr_2CO_2 and Hf_2CO_2 are very similar, in particular the bottom(top) of the conduction(valence) band. The bottom of the conduction band of Ti_2CO_2 is flatter compared to the rest.

[a] Department of Physics, Indian Institute of Technology Guwahati, Guwahati-781039, Assam, India E-mail: subhra@iitg.ac.in

† Electronic Supplementary Information (ESI) available: [details of any supplementary information available should be included here]. See DOI: 00.0000/00000000.

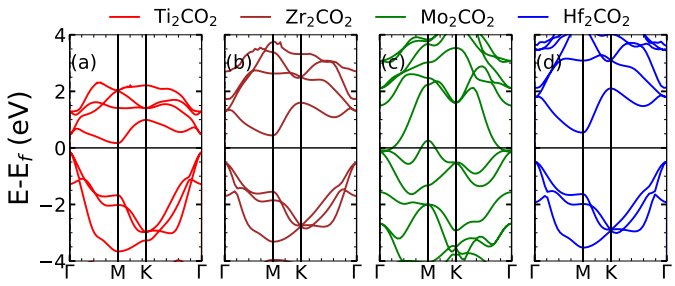

Fig. S3 Band structures of M_2CO_2 MXenes considered in this work.

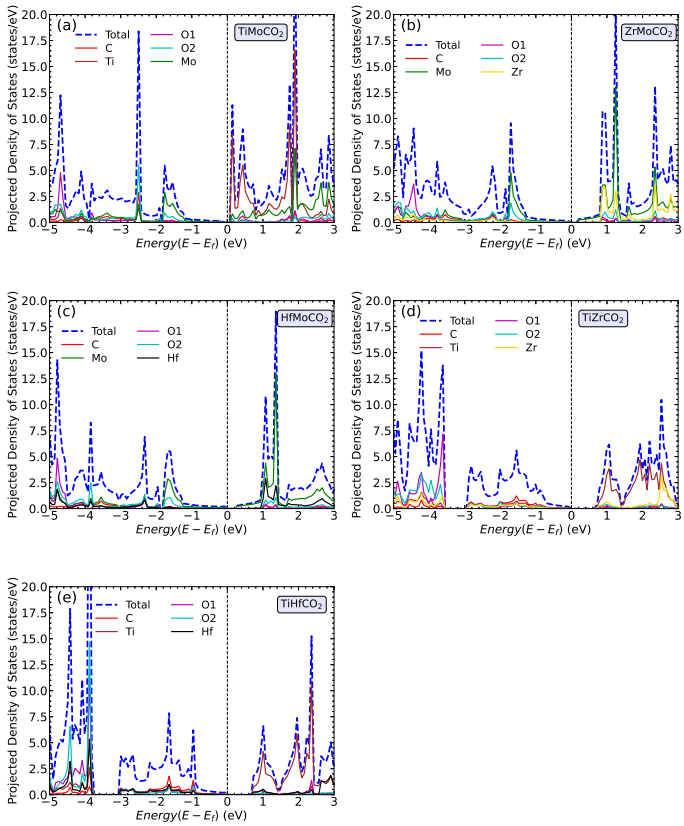

Fig. S4 Densities of States of the Janus MXenes considered.

.

Fig. S4 shows the densities of states of the Janus MXenes considered in this work. Distinct Van Hove singularity in the bottom of the conduction band is observed only in $TiMoCo_2$. This results in flattest bottom of the conduction band and large electron effective mass.

3 Phonon Spectra and Modes of vibrations

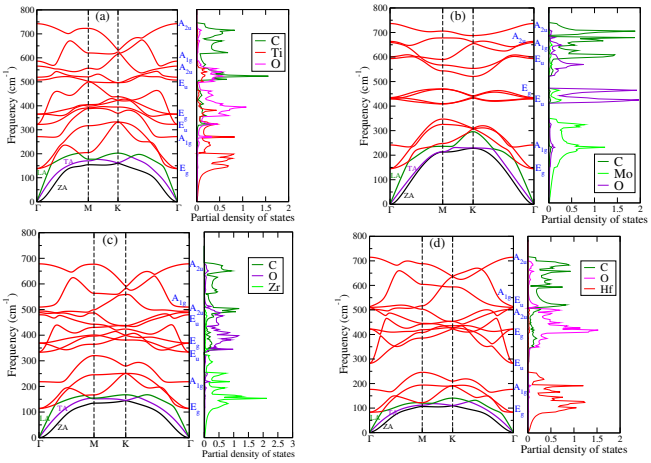

Fig. S5 Phonon spectra and densities of states of M_2CO_2 MXenes considered.

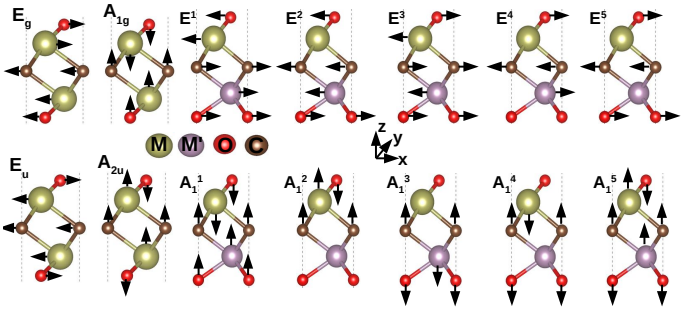

Fig. S6 Schematic diagram of phonon mode vibration at Γ point for different frequencies

In Fig. S5 and S6, phonon spectra along with atom-projected phonon densities of states of M_2CO_2 MXenes and displacement patterns associated with different vibrational modes in parent M_2CO_2 and Janus $MM'CO_2$ compounds are shown, respectively. It is evident from the phonon spectra that acoustic and optical modes are most(least) interactive in Ti_2CO_2 (Mo_2CO_2). Symmetry lowering of M_2CO_2 is achieved by forming Janus. The degeneracies in the vibrational modes are consequently lifted in Janus $MM'CO_2$. The displacement patterns in Fig. S6 demonstrate this.

4 Transport parameters

Table S2 lists the quantities required to compute the thermoelectric parameters of MXenes considered in this work. All quantities are calculated within DP approximation. In this approximation, the carrier relaxation time (τ) and carrier mobility (μ) are connected as $\tau = \frac{\mu m^*}{e}$. The carrier mobility can be obtained from $\mu = \frac{2e\hbar^3 C_{2D}}{3k_B T|m^*|^2 E_D^2}$, where e is the electron charge, m^* is carrier (electron or hole) effective mass, C_{2D} the in-plane stiffness, E_D the deformation potential constant, $\hbar$ the reduced Planck's constant, k_B the Boltzmann's constant and T is the temperature. The in-plane stiffness is calculated as $C_{2D} = \frac{1}{S_o}(\frac{\partial^2 E}{\partial \delta^2})$, where $\delta = \frac{\Delta a}{a_o}$ is the small biaxial strain applied (-1.5% to 1.5%), where S_o and a_o are the equilibrium surface area and lattice constant. The DP constant

System	Carrier	m^*/m_0	$E_d(eV)$	$C_{2D}(N/m)$	$\mu(10^4 cm^2V^{-1}s^{-1})$			$\tau(fs)$		
					$T=300K$	$T=500K$	$T=800K$	$T=300K$	$T=500K$	$T=800K$
Ti_2CO_2	e	0.408	11.39	713.02	0.0466	0.0280	0.0175	108.26	64.96	40.59
	h	0.190	3.37		2.4579	1.4747	0.9217	2655.73	1593.44	995.89
Zr_2CO_2	e	0.310	13.94	692.76	0.0524	0.0314	0.0196	92.42	55.45	34.66
	h	0.404	6.48		0.1428	0.0857	0.0535	328.21	196.92	123.08
Hf_2CO_2	e	0.257	13.59	732.73	0.0849	0.0509	0.0318	124.07	74.44	46.53
	h	0.439	5.65		0.1683	0.1009	0.0631	420.22	252.13	157.58
$TiMoCO_2$	e	2.14	1.97	866.32	0.0689	0.0413	0.0258	838.35	503.014	314.383
	h	0.31	8.48		0.1818	0.1091	0.0682	316.42	189.85	118.65
$ZrMoCO_2$	e	0.44	4.32	783.51	0.3135	0.1881	0.1176	775.68	465.41	290.88
	h	0.46	8.48		0.0721	0.0432	0.0270	189.54	113.72	71.08
$HfMoCO_2$	e	0.43	6.02	821.10	0.1708	0.1024	0.0640	420.54	252.32	157.70
	h	0.53	7.50		0.0721	0.0432	0.0270	219.29	131.57	82.23
$TiZrCO_2$	e	0.46	11.77	680.28	0.0316	0.0190	0.0118	84.33	50.59	31.62
	h	0.29	4.35		0.5683	0.3410	0.2131	966.35	579.81	362.38
$TiHfCO_2$	e	0.44	12.45	704.64	0.0336	0.0201	0.0126	83.61	50.16	31.35
	h	0.29	5.34		0.3959	0.2375	0.1484	668.69	401.21	250.76

Table S2 Effective mass(m^*), DP constant(E_d), In-plane stiffness(C_{2D}), Carrier mobility(μ) and Relaxation times(τ) of electrons and holes for the compounds considered in this work.

$E_D = \frac{\partial E_{edge}}{\partial \delta}$, where E_{edge} is the valence or conduction band edges, depicts how the conduction or valence band edge shifts under applied strain. The shift with respect to the strain is linearly fitted and E_D is obtained from the slope of the fit. The carrier effective mass is given as $m^* = \hbar^2 \left[\frac{\partial^2 E(k)}{\partial k^2}\right]^{-1}$; k and $E(k)$ are the wave vector and the corresponding band energy, respectively. The effective masses reported in this work are the ones at the band edges, obtained by fitting the band edge energies. In case of degenerate or quasi-degenerate bands at the edges, as seen in cases of valence bands in $TiZrCO_2$ and $TiHfCO_2$ (Figures 2(d) and 2(e), main paper), $E(k)$ corresponding to the flatter band is considered. This yields the larger m^*. In case of band edges being parabolic, the fitting is done through a quadratic function,

$$E(k) = \frac{\hbar^2 k^2}{2m^*} \tag{1}$$

For the non-parabolic band edges, the Kane quasi-linear band dispersion is considered [1] for the fitting,

$$E(1+\alpha E) = \frac{\hbar^2 k^2}{2m^*} \tag{2}$$

where α is the measure of departure from parabolic nature due to flattening of bands. For a parabolic band, $\alpha = 0$ while for a non-parabolic conduction(valence) band $\alpha > (<) 0$. Using the nonlinear least square curve fitting the α value is optimised to minimize the difference between the Kane quasi-linear band dispersion (Eq. 2) and DFT evaluated band energies. Once the optimal value of α is obtained, the effective mass is evaluated.

Fig. S7 and S8 show the phonon group velocities in M_2CO_2 and $MM'CO_2$ MXenes, respectively. Largest group velocities, in all cases, are obtained for low lying acoustic modes.

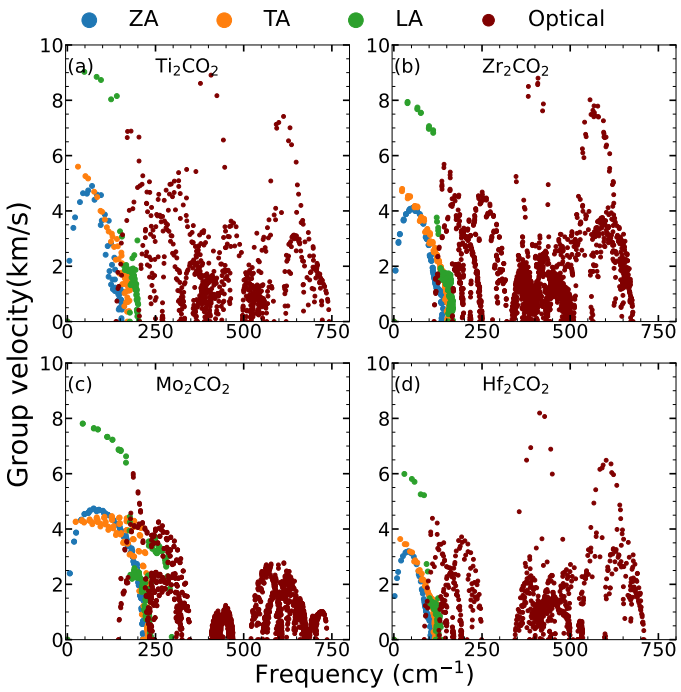

Fig. S7 Group velocities of phonon modes in M_2CO_2 MXenes. Blue, orange, green, and brown colors indicate the ZA, TA, LA, and optical modes, respectively

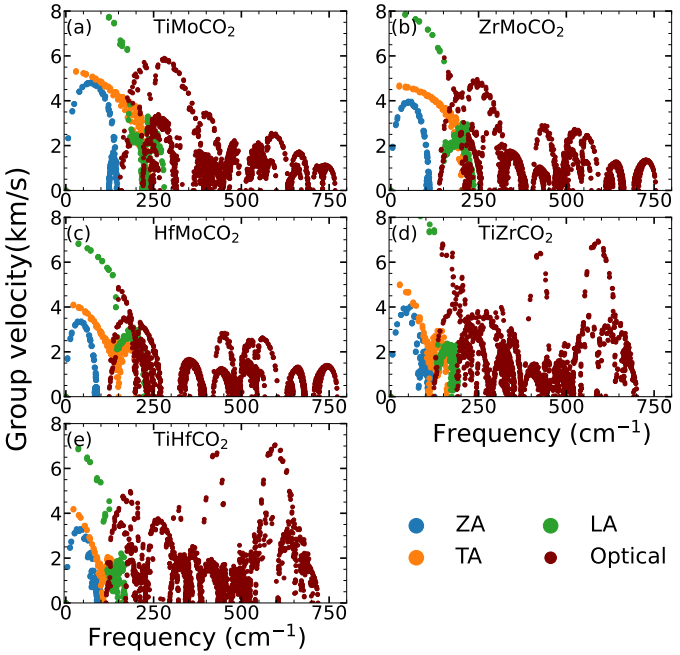

Fig. S8 Group velocities of phonon modes in $MM'CO_2$ Janus MXenes. Blue, orange, green, and brown colors indicate the ZA, TA, LA, and optical modes, respectively

Fig. S9 shows the normalised cumulative lattice thermal conductivity as a function of frequency in the MXenes considered in this work.

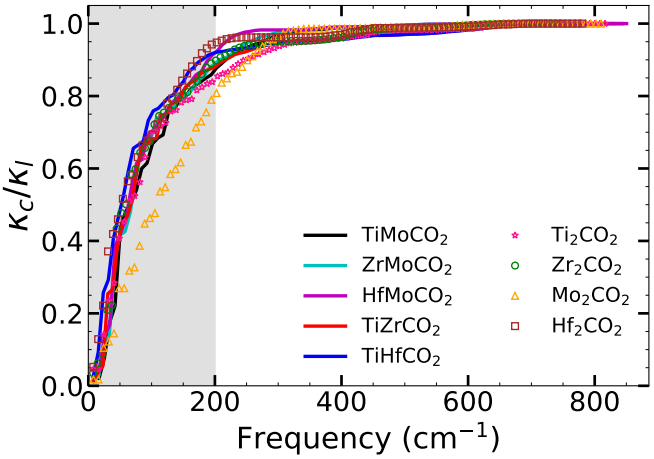

Fig. S9 Normalised cumulative lattice thermal conductivity as a function of frequency for the MXenes considered.

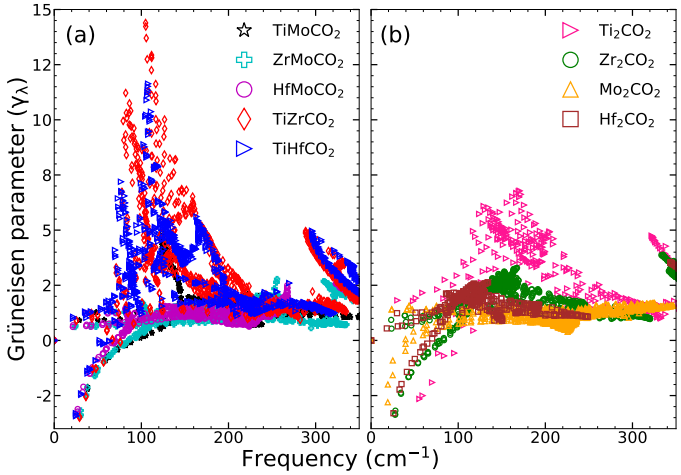

Fig. S10 Grüneisen parameter for the (a) Janus and (b) parent MXenes considered.

Fig. S10 shows the variations in the mode Grüneisen parameter for the MXenes. The range of frequency in which contributions to κ_l is maximum, is considered. We find that Janus MXenes are more anharmonic than the corresponding parent MXenes.

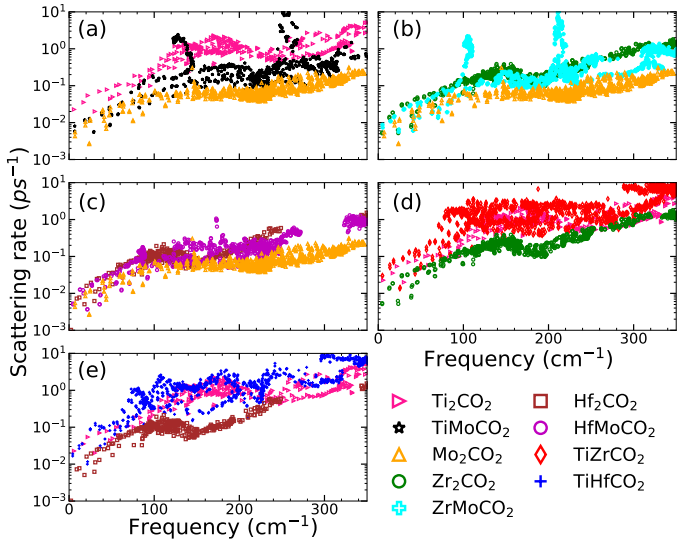

Fig. S11 Comparison of anharmonic scattering rates between Janus and corresponding parent MXenes.

Fig. S11 shows a comparison of phonon-phonon scattering rates for a given Janus and the corresponding parent MXenes. For non-Mo Janus, the scattering rate in Janus is more than either parents.

Notes and references

1 L. D. Whalley, J. M. Frost, B. J. Morgan and A. Walsh, *Phys. Rev. B*, 2019, **99**, 085207.